IRS-Assisted High-Speed Train Communications: Performance Analysis and Optimal Configuration

Meilin Gao, *Member, IEEE*, Bo Ai, *Fellow, IEEE*, Yong Niu, *Senior Member, IEEE*, Qihao Li, *Member, IEEE*, Zhu Han, *Fellow, IEEE*, Zhangdui Zhong, *Fellow, IEEE*, Xuemin Shen, *Fellow, IEEE*, and Ning Wang, *Member, IEEE*

***Abstract*—High-speed train (HST) communications are envisioned to provide diversified broadband services by integrating with 5G while the high mobility induces fast-fading channels and potentially degrades the system performance. To address this issue, we investigate an HST communication network empowered by intelligent reflecting surfaces (IRSs) with the multiple-input–multiple-output (MIMO) technology. Statistical channel state information (CSI) is exploited to mitigate the impact of the fast time-varying fading. The transceiver beamforming vectors and the IRS phase shift matrix are optimized to improve the system performance in terms of the outage probability and the ergodic capacity considering the channel uncertainty. First, we derive the analytical expression of the outage probability with a generalized Marcum *Q*-function. Then, we develop an alternating optimization algorithm to minimize the outage probability by capitalizing on the generalized eigenvalue–eigenvectors. Moreover, the ergodic capacity is deduced with statistical CSI and then optimized by analyzing the upper bound with Jensen's approximation. Extensive simulations show that simulation results are consistent with the theoretical analysis, and the IRS-assisted system significantly outperforms the system without IRS in terms of the outage probability and the ergodic capacity.**

***Index Terms*—Ergodic capacity, high-speed train (HST) communications, intelligent reflecting surface (IRS), outage probability, statistical channel state information (CSI).**

Manuscript received 17 November 2022; revised 25 February 2023; accepted 24 March 2023. Date of publication 10 April 2023; date of current version 24 October 2023. This work was supported in part by the National Key Research and Development Program under Grant 2020YFB1806604, Grant 2021YFB2900301, and Grant 2021YFB3901302; in part by the National Natural Science Foundation of China under Grant 62231009 and Grant 62221001; in part by the Royal Society Newton Advanced Fellowship under Grant NA191006 and Grant 61961130391; in part by the Open Research Fund from the Shenzhen Research Institute of Big Data under Grant 2019ORF01006; in part by the National Key Research and Development Program of China under Grant 2020YFB1806903; in part by NSF under Grant CNS-2107216, Grant CNS-2128368, and Grant CMMI-2222810; in part by the U.S. Department of Transportation; in part by Toyota; and in part by Amazon. *(Corresponding author: Bo Ai.)*

Meilin Gao is with the Beijing National Research Center for Information Science and Technology, Tsinghua University, Beijing 100084, China (e-mail: gao_meilin@163.com).

Bo Ai is with the State Key Laboratory of Rail Traffic Control and Safety, Beijing Jiaotong University, Beijing 100044, China, and also with the Peng Cheng Laboratory, Shenzhen 518055, China (e-mail: boai@bjtu.edu.cn).

Yong Niu is with the State Key Laboratory of Rail Traffic Control and Safety, Beijing Jiaotong University, Beijing 100044, China, and also with the National Mobile Communications Research Laboratory, Southeast University, Nanjing 211189, China (e-mail: niuy11@163.com).

Qihao Li is with the School of Electrical Engineering and Intelligentization, Dongguan University of Technology, Dongguan 523000, Guangdong, China (e-mail: qihao.li@ieee.org).

Zhu Han is with the Department of Electrical and Computer Engineering, University of Houston, Houston, TX 77004 USA, and also with the Department of Computer Science and Engineering, Kyung Hee University, Seoul 446-701, South Korea (e-mail: hanzhu22@gmail.com).

Zhangdui Zhong is with the State Key Laboratory of Rail Traffic Control and Safety, Beijing Jiaotong University, Beijing 100044, China (e-mail: zhdzhong@bjtu.edu.cn).

Xuemin Shen is with the Department of ECE, University of Waterloo, Waterloo, ON N2L 3G1, Canada (e-mail: sshen@uwaterloo.ca).

Ning Wang is with the School of Information Engineering, Zhengzhou University, Zhengzhou 450001, China (e-mail: ienwang@zzu.edu.cn).

Digital Object Identifier 10.1109/JIOT.2023.3265655

I. Introduction

HIGH-SPEED train (HST) communication networks are envisioned to provide more diverse data-immense services, including automatic train operation, Internet of Things for railways and passenger infotainment, for HST operating beyond 350 km/h with ambitious data rates reaching multi-gigabits per second [2]. Millimeter-wave (mmWave) technologies with frequencies ranging from 30 to 300 GHz have been investigated to meet the immense demands for higher data rates [3], which serves as a powerful engine to enhance the train-to-ground capacity. Several challenges faced with mmWave technologies include blockage sensitivity, propagation attenuation and penetration loss [4]. Unfortunately, blockage widely exists in HST environments, where random obstructions are distributed along the rail track, such as transportation infrastructure [5].

Intelligent reflecting surface (IRS) has been exploited to combat the blockage issue and improve the link transmission quality by providing assistant Line-of-Sight (LoS) link connections [6]. IRS is capable of reconfigurable electromagnetic (EM) features including the phase shift control of each reflecting element in real time. In general, IRS is dynamically implemented by tuning PIN diodes via the bias voltages and is generally connected to a central controller in a field-programmable gate array (FPGA) [7]. Therefore, IRS can manipulate the incident EM wave propagation to the target direction and rebuild wireless channel environments to be favorable. Specifically, IRS can be integrated with the multiple-input–multiple-output (MIMO) technology and serve as passive beamforming by adjusting the phase shift and amplitude of all reflecting elements.

To meet the performance requirements of IRS-assisted HST communication networks, several intrinsic challenges should

be addressed. First, due to the high mobility of the train and nearly passive capability of IRSs, the instantaneous channel state information (CSI) in the considered network is difficult to acquire thus may affecting the system performance [1]. For one thing, high-mobility communications introduce fast fading which incurs frequent channel measurement and heavy feedback burden. The fast time-varying fading may deteriorate the detection accuracy of instantaneous CSI due to the rapid channel variation [8]. The system performance will be degraded if the beamforming configuration is designed adaptive to inaccurate CSI. For another, IRS is generally considered to be passive without channel sensing capability. It is power consuming and inefficient to frequently update IRS reflecting coefficients with instantaneous CSI in a short stationarity time.

Second, it is difficult to derive explicit expressions while characterizing outage probability and ergodic capacity [9]. Rician scenarios happen when the train travels at high speeds and concurrently receives signals from the trackside base stations (BSs) and the IRSs. Therefore, the composite wireless channel conforms to a finite sum representation of the Gaussian cumulative distribution function (CDF) complicates the expression derivation. In this particular IRS-assisted HST MIMO communication system, it is necessary to approximate the nonconvexity function into an explicit and tractable function to make the optimization problem easy to solve.

Third, traditional optimization such as the nonlinear programming technique incurs excessively high computational complexity, which is proportional to the number of transceiver antennas and IRS elements since it involves huge search operations for possible action space. Nevertheless, this work is confined to an HST mmWave MIMO scenario enhanced by IRS implementation. It is necessary to find an efficient solution to optimize the approximated explicit functions.

Motivated by the above challenges, we study the performance analysis and optimal configuration of the IRS-assisted downlink MIMO system for HST communications composing direct and reflective connections, by utilizing the slow-varying statistical CSI with location-related information. All channels associated with the train are modeled as Rician fading channels since both LoS and non-LoS components exist most of the time. Specifically, we investigate the optimal design of the transceiver beamforming and IRS phase shift matrix, then propose cost-effective solutions to address the above challenges while determining the optimal configuration. The following are the main contributions of this article.

1) We integrate IRSs into HST MIMO systems to address the blockage issue of signal transmission. Moreover, we utilize statistical CSI of the involved transmission channels to reduce the impact of fast fading channels induced by the high mobility and avoid the heavy overheads when exploring and exploiting instantaneous CSI.
2) We employ a generalized Marcum Q-function to approximate the derived closed-form expression of the outage probability with statistical CSI to make it tractable. Then, we develop an alternating optimization algorithm to solve the outage probability minimization problem with the generalized eigenvalue–eigenvectors and quadratically constrained quadratic programming (QCQP).
3) We investigate the ergodic capacity in terms of the channel uncertainty and analyze the upper bound and Jensen's approximation since the nonconvex ergodic capacity maximization problem is difficult to be directly solved. A computationally effective algorithm is designed to tackle the time-consuming problem and optimize the upper bound of the ergodic capacity approximation.

The remainder of this article is organized as follows. Section II presents related works. Section III describes the system model. In Section IV, we formulate the outage probability minimization problem and present an algorithm with statistical CSI. In Section V, we investigate the ergodic capacity maximization problem and derive the upper bound and Jensen's approximation. Numerical results are presented in Section VI to evaluate the proposed algorithms. Finally, Section VII concludes this work.

II. Related Work

The blockage problem has been studied with massive MIMO technology, such as relay-assisted cooperation systems and large-scale antenna systems [10], [11]. On the one hand, the relay-assisted schemes steer signal transmissions around obstacles by multihop forwarding [12]. However, the relay not only consumes power to amplify (or decode) and forward signals but also operates in either half-duplex (thus lowering efficiency) or full-duplex (thus introducing self-interference) mode [13]. On the other hand, the large-scale antenna system is developed as massive MIMO to remedy the blockage issue and signal attenuation by steering narrow beams with substantial beamforming gains [14]. But the large-scale antenna systems suffer from huge path loss and penetration loss when confronted with poor wireless propagation conditions such as in high-mobility scenarios. Some of the existing anti-blockage schemes are expensive to be implemented in outdoor scenarios due to the expenditure of extensive backup access points and/or BS deployment.

To remedy the above limitations, IRS has been exploited to enhance wireless communications in a cost-effective way, particularly when the LoS connection between the transceiver is weak or interrupted. IRS has been regarded as not only an alternative to typical phased arrays but also as a new paradigm for IRS-assisted communication systems that have recently attracted substantial research attention. In [15], an IRS-aided multiuser communication network is studied in a multiple-user multiple-input single-output (MU-MISO) scenario, and the power consumption is minimized by utilizing an alternation optimization. In [16], IRS is utilized to mitigate mutual interference in device-to-device communications and maximize the sum rate with a suboptimal solution. However, the instantaneous CSI is assumed to be available [15], [16], and this may not be proper in high-mobility scenarios. In addition, updating the IRS reflecting coefficients regularly with instantaneous CSI is inefficient and power consuming.

In the case of an IRS-aided system without instantaneous CSI, numerous research efforts have been devoted to channel

estimation [17], [18], [19], [20]. These channel estimation strategies can be divided into following main categories. First, ON–OFF based channel estimation schemes are executed by sequentially tuning on a single IRS element (or a combination of IRS elements) or by evaluating the direct link and all reflected links one by one [17], [18]. Second, overheads-aware efficient schemes are developed by utilizing compressing sensing or deep learning [19], [20]. Inevitable estimation errors arise from limited channel measurements (in terms of power, frequency, or time) and impractical assumptions (including sparse characteristics), thus affecting the system performance. In view of above challenges, statistical CSI which varies more slowly than instantaneous CSI and can be comparatively easily explored is beneficial for high-mobility scenarios. Depending on the deterministic large-scale information, statistical CSI (including spatial correlation and channel covariance) remains invariant for a longer interval. Thus it is reasonable for BSs to exploit slow varying statistical CSI via long-term feedback and covariance extrapolation [1]. Generally, statistical CSI is more accessible in high-speed railways since the commuting route and location information are available.

Recently, some works advocate the utilization of IRS in high-mobility scenarios [21], [22], [23], [24], [25], [26], [27], with an emphasis on numerous categories, such as IRS configuration [22], [23], channel estimation [24], [25], and performance analysis [26], [27]. In [21], an IRS-aided HST communication paradigm depicting key challenges and main application scenarios is elaborated, and it also provides promising solutions and points out future directions. The joint configuration of IRS phase shift and transceiver beamforming in an HST MIMO system is investigated in [22] to maximize the ergodic capacity by an alternative optimization algorithm, assuming the direct link and reflection link coexist while one is for communication and the other one is for measurement. Against outdated CSI, a deep reinforcement learning approach is developed in [23] to orchestrate the IRS phase shift and transceiver beamforming to improve the spectral efficiency in an IRS-aided HST MISO system. In [24], a practical channel estimation framework is designed for the HST MIMO system aided by both onboard and roadside IRSs. In [25], IRS is employed in high-speed vehicular communications and a two-stage transmission protocol is proposed to achieve both IRS channel estimation and refraction optimization. In [26], a continuous time propagation model in IRS-assisted low-Earth-orbit (LEO) satellite communications is developed with predictive mobility compensation. In [27], IRS is introduced into an HST SISO system to suppress interference from EM disturbances or other communications systems.

Aforementioned works provide interesting results but pay little attention to the HST MIMO system especially when CSI is unavailable and both direct link and reflection links are considered for communications. Questions remain open regarding the outage probability minimization problem and approximating the ergodic capacity. In this article, we aim to reduce the outage probability and increase the ergodic capacity under the assumption of statistical CSI for HST MIMO communications.

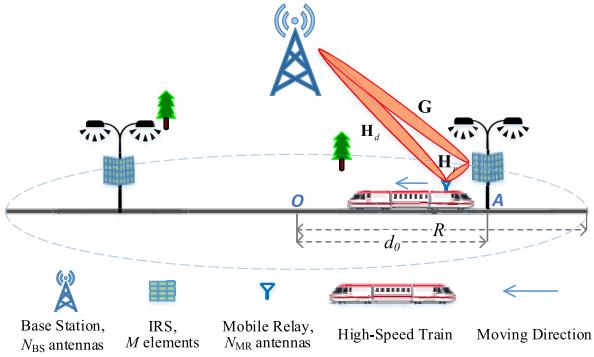

Fig. 1. Illustration of an IRS-assisted system for HST communications.

III. System Model

In this section, we elaborate an IRS-assisted HST communication system as sketched in Fig. 1.

A. IRS-Assisted Architecture for HST Communications

In the considered system, a trackside BS serves the users onboard the HST during the dwelling time. A mobile relay (MR) is installed on top of the train to reduce penetration loss and frequent handover. The BS and the MR are equipped with N_{BS} and N_{MR} antennas, respectively. Two IRSs are centered around the BS along the rail track, to rebuild reflection links. Each IRS comprises a smart controller connected to the BS via a wired way. IRSs are composed of M passive reflecting elements to alter the amplitude and phase shifts in incident signals, thus regulating radio propagation into target directions. There is only one IRS activated by the BS through the controller to communicate with the MR, which depends on the train's current location. If the train resides on the left side of the cell coverage, the IRS on the left is accordingly chosen to serve as a passive relay while the right-side IRS is muted. Otherwise, the left-side IRS is muted while the right-side IRS is activated as the passive relay. As shown in Fig. 1, the projections of the BS and the serving IRS onto the track are denoted as points O and A. The horizontal distance between BS and IRS is denoted as d_0 and the cell radius is denoted as R, while d_0 ranges from 0 to R.

For practical application, the time of IRS phase shift operation T_o depends on the EM pulse according to the regulation voltage, which is in orders of ns [28]. To measure the time-variant effect in HST communications, the stationarity time is introduced during which time the channel keeps constant or has no great change. T_s is in orders of milliseconds in HST mmWave communications [29]. Thus it is valid and practical for the almost real-time IRS operation in time-varying HST communications.

The transmitted symbol from the BS to the MR is denoted by $x \in \mathbb{C}$. Without loss of generality, we assume $\mathbb{E}\{x\} = 0$ and $\mathbb{E}\{x^H x\} = 1$. The BS adopts the transmit beamforming vector $\boldsymbol{f} \in \mathbb{C}^{N_{\mathrm{BS}} \times 1}$ to transmit the symbol x, where the transmit power constraint should be satisfied as $\|\boldsymbol{f}\|^2 \leq P_T$ and $\|\cdot\|$ denotes the Euclidean norm. Similarly, the MR adopts the combing vector $\boldsymbol{\omega} \in \mathbb{C}^{N_{\mathrm{MR}} \times 1}$. The channel matrices of the direct link from the BS to the MR, of the reflection link from the IRS to the MR,

and of the link from the BS to the IRS are denoted by $H_d \in \mathbb{C}^{N_{\mathrm{BS}} \times N_{\mathrm{MR}}}$, $H_r \in \mathbb{C}^{M \times N_{\mathrm{MR}}}$, and $G \in \mathbb{C}^{M \times N_{\mathrm{BS}}}$, respectively. Note that all involved links are assumed for communications to improve the system throughput.

The reflection-coefficient matrix of the IRS is denoted as a diagonal matrix $\boldsymbol{\Theta} = \mathrm{diag}(\theta_1, \ldots, \theta_m, \ldots, \theta_M)$. Herein, $\theta_m = \beta_m e^{j\epsilon_m}$ is composed of the amplitude reflection coefficient $\beta_m \in [0, 1]$ and the phase-shift coefficient $\epsilon_m \in [0, 2\pi)$. j is the imaginary unit. Ideal reflection is widely assumed for all elements of IRSs with $\beta_m = 1$ and $|\theta_m|^2 = 1$ [15].

The signal received at the MR is expressed as

$$y = \underbrace{\boldsymbol{\omega}^H \left(H_d^H + H_r^H \boldsymbol{\Theta} G\right) \boldsymbol{f} x}_{\text{the desired signal}} + \boldsymbol{\omega}^H \boldsymbol{n} \tag{1}$$

where $\boldsymbol{n}$ is the additive white Gaussian noise at the MR with distribution $\mathcal{CN}(\mathbf{0}, \sigma^2 \mathbf{I}_{N_{\mathrm{MR}}})$.

Hence, the signal-to-noise ratio (SNR) at the MR is

$$\gamma = \frac{|\boldsymbol{\omega}^H \left(H_d^H + H_r^H \boldsymbol{\Theta} G\right) \boldsymbol{f}|^2}{\sigma^2} \tag{2}$$

where $|\cdot|$ denotes the modulus.

B. Channel Model

Given the stationary of the predeployed BS and IRSs, G can be precisely acquired by the BS in advance. Due to the high velocity of the train, both H_d and H_r related with the train vary with time and transceiver distance.

We describe the time-varying characteristics of channels H_d and H_r using the Rician fading model, where NLoS components vary slowly and LoS components are location-based [30]. Specifically, H_d is modeled as

$$H_d = \sqrt{\frac{\kappa_d}{\kappa_d + 1}} \bar{H}_d + \sqrt{\frac{1}{\kappa_d + 1}} \tilde{H}_d \tag{3}$$

where $\bar{H}_d$ represents the LoS components of the direct link which stays constant in the channel coherence time, $\tilde{H}_d$ represents the NLoS components which entity is modeled as an independent circularly symmetric complex Gaussian (CSCG) random variable with $\mathcal{CN}(0, \sigma_d^2)$, and κ_d is the Rician K-factor of H_d. The Rician K-factor is a crucial parameter to characterize the channel quality, representing the ratio of the strength of the LoS component and the NLoS component [31]. The shadowing effect is neglected and the large-scale fading is assumed to be dependent on the path loss. As observed, this channel model converges to Rayleigh fading when $\kappa_d = 0$ and to an LoS channel when $\kappa_d \to \infty$.

Two types of array architectures are adopted where antennas at the BS and the MR are equipped in a uniform linear array (ULA) and IRS elements are displaced in a uniform planar array (UPA). The Angle of Arrival (AoA) and the Angle of Departure (AoD) of the BS-MR direct link is respectively, denoted by ν_{MR}, φ_{BS}, and $\bar{H}_d$ is expressed as

$$\bar{H}_d = \boldsymbol{a}_r(\nu_{\mathrm{MR}}) \boldsymbol{a}_t^H(\varphi_{\mathrm{BS}}). \tag{4}$$

Similarly, we can easily model H_r as

$$H_r = \sqrt{\frac{\kappa_r}{\kappa_r + 1}} \bar{H}_r + \sqrt{\frac{1}{\kappa_r + 1}} \tilde{H}_r \tag{5}$$

where $\bar{H}_r$ ($\tilde{H}_r$) represents the LoS (NLoS) components of the reflection link, respectively. κ_r is the Rician K-factor of H_r. Similarly, the entries of $\tilde{H}_r$ are independently generated from CSCG distribution $\mathcal{CN}(0, \sigma_r^2)$. The antennas at the MR are arranged in a ULA mode, thus $\bar{H}_r$ follows the similar form as (4) and is omitted for short.

The elements of the IRS are supposed to form a UPA structure and the BS-IRS channel G is modeled by

$$\begin{aligned} G &= \boldsymbol{a}_r\left(\nu_{\mathrm{IRS},a}, \nu_{\mathrm{IRS},e}\right) \boldsymbol{a}_t^H(\vartheta_{\mathrm{BS}}) \\ &= \boldsymbol{a}_{r,a}\left(\nu_{\mathrm{IRS},a}\right) \otimes \boldsymbol{a}_{r,e}^H\left(\nu_{\mathrm{IRS},e}\right) \boldsymbol{a}_t^H(\vartheta_{\mathrm{BS}}) \end{aligned} \tag{6}$$

where $\otimes$ is the Kronecker product, $\nu_{\mathrm{IRS},a}$ ($\nu_{\mathrm{IRS},e}$) and ϑ_{BS} represent the azimuth (elevation) AoA and the AoD of the BS-IRS assistant link.

The composite channel H can be expressed as

$$H = H_d + G^H \boldsymbol{\Theta}^H H_r. \tag{7}$$

The LoS components $\bar{H}_d$ and $\bar{H}_r$, are dependent on the MR's location and are accessible when accurate location information of the train is available. As noted above, the BS-IRS assistant channel, G, is precisely known for fixed deployment.

IV. Outage Probability Minimization

Considering the outage probability minimization, we first deduce an explicit expression of the outage probability and then develop an outage probability minimization algorithm.

A. Outage Probability Minimization Problem Formulation

We investigate the outage probability minimization problem to find the optimal configuration of the transceiver beamforming and the IRS coefficient design, while satisfying the transmit power limit and the constant modulus constraint.

Let P_{out} denote the outage probability, which illustrates the received signal power falls below the given threshold

$$\begin{aligned} P_{\mathrm{out}} &\triangleq \Pr(\gamma \le \gamma_{th}) \\ &= \Pr\left(|\boldsymbol{\omega}^H \left(H_d^H + H_r^H \boldsymbol{\Theta} G\right) \boldsymbol{f}|^2 \le \sigma^2 \gamma_{th}\right) \end{aligned} \tag{8}$$

where γ_{th} is the corresponding SNR threshold in dB. The outage probability minimization problem is formulated as

$$\mathcal{P}1: \min_{\boldsymbol{\omega}, \boldsymbol{f}, \boldsymbol{\Theta}} \quad P_{\mathrm{out}} \tag{9a}$$

$$\text{s.t.} \quad \|\boldsymbol{f}\|^2 \le P_T \tag{9b}$$

$$\|\boldsymbol{\omega}\|^2 \le 1 \tag{9c}$$

$$|\theta_m|^2 = 1 \ \forall m \in \{1, \ldots, M\} \tag{9d}$$

where P_T denotes the transmit power limit. The problem is intangible because it is prohibitive to obtain a tractable or analytical closed-form expression for the probability function in (9a) and the unit-modulus constraint in (9d) is nonconvex. To solve the problem, we first derive the outage probability distribution with the location-dependent statistical CSI, then reformulate the objective function.

B. Outage Probability Analysis

This section first features the outage probability by analyzing properties of the composite channel, then transforms the implicit objective function (9a) into an explicit representation.

Proposition 1: Each element of the composite channel H obeys a complex Gaussian distribution, i.e., $H_{i,j} \sim \mathcal{CN}(\mu_{i,j}, \sigma_{i,j}^2)$ wherein the mean value $\mu_{i,j}$ and the variance $\sigma_{i,j}^2$ can be given by

$$\mu_{i,j} = \alpha_d\left(\bar{H}_d\right)_{i,j} + \alpha_r\left(G^H\boldsymbol{\Theta}^H\bar{H}_r\right)_{i,j} \tag{10a}$$

$$\sigma_{i,j}^2 = \beta_d^2\sigma_d^2 + \beta_r^2\|G_{(:,i)}\|^2\sigma_r^2 \tag{10b}$$

where $\alpha_d = \sqrt{(\kappa_d/[\kappa_d+1])}$, $\beta_d = \sqrt{(1/[\kappa_d+1])}$, $\alpha_r = \sqrt{(\kappa_r/[\kappa_r+1])}$, and $\beta_r = \sqrt{(1/[\kappa_r+1])}$.

Proof: The detailed proof is given in Appendix A. ■

Specifically, $\bar{H} \triangleq \mathbb{E}\{H\} = \alpha_d\bar{H}_d + \alpha_r G^H\Theta^H\bar{H}_r$, $\bar{H}_{i,j} = \mu_{i,j}$, where $\mathbb{E}\{\cdot\}$ is the expectation operator. In the following, the derivation of the desired signal received at the MR to an amiable form helps gain insights into the problem.

Proposition 2: The term $X = \boldsymbol{f}^H H\boldsymbol{\omega}$ follows a complex Gaussian distribution, i.e., $X \sim \mathcal{CN}(\mu_X, \sigma_X^2)$ with mean μ_X and variance σ_X^2 given by

$$\mu_X = \boldsymbol{f}^H\bar{H}\boldsymbol{\omega}, \quad \sigma_X^2 = \boldsymbol{f}^H\Omega_1\boldsymbol{f} = \boldsymbol{\omega}^H\Omega_2\boldsymbol{\omega} \tag{11}$$

where we invite two auxiliary variables

$$\Omega_1 = \mathrm{diag}(\boldsymbol{\varpi}), (\boldsymbol{\varpi})_i = \sum_{j=1}^{N_{\mathrm{MR}}}\sigma_{i,j}^2|\omega_j|^2, \ \forall i \in \{1,\ldots,N_{\mathrm{BS}}\}$$

$$\Omega_2 = \mathrm{diag}(\boldsymbol{\varrho}), (\boldsymbol{\varrho})_j = \sum_{i=1}^{N_{\mathrm{BS}}}\sigma_{i,j}^2|f_i|^2, \ \forall j \in \{1,\ldots,N_{\mathrm{MR}}\}. \tag{12}$$

Proof: The detailed proof is given in Appendix B. ■

Based on the analysis above, the distribution of the outage probability can be derived by manipulating the statistical CSI in the following proposition.

Proposition 3: The outage probability in the considered system is derived by a noncentral chi-square distribution $\chi^2(\upsilon, \lambda)$ with 2 degrees of freedom and noncentrality parameter $\lambda = (\mu_X^2/\sigma_X^2)$. The outage probability can be derived as follows:

$$P_{out} = 1 - Q_{\frac{\upsilon}{2}}\left(\sqrt{\lambda}, \sqrt{\gamma_0}\right) \tag{13}$$

where $\gamma_0 = (\sigma^2\gamma_{th}/\sigma_X^2)$ and $Q_M(a,b)$ is the generalized (Mth-order) Marcum Q-function.

Proof: With Proposition 2, $(X/\sigma_X) \sim \mathcal{CN}([\mu_X/\sigma_X], 1)$. Therefore, $Y = |(X/\sigma_X)|^2 = |([\boldsymbol{f}^H H\boldsymbol{\omega}]/\sigma_X)|^2$ obeys a chi-square distribution, i.e., $Y \sim \chi^2(\upsilon, \lambda)$ with the degree of freedom $\upsilon = 2$ since one for the real part and one for the image part [32]. The noncentrality parameter λ is given by

$$\lambda = \frac{\mu_X^2}{\sigma_X^2} = \frac{|\boldsymbol{f}^H\bar{H}\boldsymbol{\omega}|^2}{\boldsymbol{f}^H\Omega_1\boldsymbol{f}} = \frac{|\boldsymbol{f}^H\bar{H}\boldsymbol{\omega}|^2}{\boldsymbol{\omega}^H\Omega_2\boldsymbol{\omega}} = \frac{\boldsymbol{f}^H\Xi_1\boldsymbol{f}}{\boldsymbol{f}^H\Omega_1\boldsymbol{f}} = \frac{\boldsymbol{\omega}^H\Xi_2\boldsymbol{\omega}}{\boldsymbol{\omega}^H\Omega_2\boldsymbol{\omega}} \geq 0 \tag{14}$$

where $\Xi_1 = \bar{H}\boldsymbol{\omega}\boldsymbol{\omega}^H\bar{H}^H$ and $\Xi_2 = \bar{H}^H\boldsymbol{f}\boldsymbol{f}^H\bar{H}$. A central chi-square distribution is a special case of the chi-square distribution defined above with $\lambda = 0$, whereas in practical IRS-assisted HST communications $\lambda > 0$ leads to a noncentral chi-square distribution.

The outage probability defined in (8) is easily shown to be

$$\begin{aligned} P_{\mathrm{out}} &= \Pr\left(|\boldsymbol{\omega}^H\left(H_d^H + H_r^H\boldsymbol{\Theta}G\right)\boldsymbol{f}|^2 \leq \sigma^2\gamma_{th}\right) \\ &= \Pr\left(\left|\frac{\boldsymbol{f}^H H\boldsymbol{\omega}}{\sigma_X}\right|^2 \leq \frac{\sigma^2\gamma_{th}}{\sigma_X^2}\right) = F_{\upsilon,\gamma_0}(Y) \end{aligned} \tag{15}$$

where $\gamma_0 = ([\sigma^2\gamma_{th}]/\sigma_X^2)$, and $F_{\upsilon,\gamma_0}(Y)$ denote the CDF of the noncentral chi-square distribution $Y \sim \chi^2(\upsilon, \lambda)$. Using the CDF of the noncentral chi-square distribution [33], we have

$$P_{\mathrm{out}} = 1 - Q_{\frac{\upsilon}{2}}\left(\sqrt{\lambda}, \sqrt{\gamma_0}\right) \tag{16}$$

where $Q_M(a,b)$ is the generalized Marcum Q-function of real order M. ■

The generalized Marcum Q-function $Q_M(a,b)$ is log-concave and monotonically increasing with regard to both a and b [34, p. 451]. Further exploiting the monotonicity of Proposition 3, the following implication holds true:

$$\min_{\boldsymbol{\omega},\boldsymbol{f},\boldsymbol{\Theta}} \ P_{\mathrm{out}} = 1 - Q_1\left(\sqrt{\lambda}, \sqrt{\gamma_0}\right) \ \Leftrightarrow \ \max_{\boldsymbol{\omega},\boldsymbol{f},\boldsymbol{\Theta}} \ \lambda. \tag{17}$$

Applying (17) to $\mathcal{P}1$ gives rise to the following problem:

$$\begin{aligned} \mathcal{P}2: \ \max_{\boldsymbol{\omega},\boldsymbol{f},\boldsymbol{\Theta}} \ & \frac{\mu_X^2}{\sigma_X^2} = \frac{|\boldsymbol{f}^H\bar{H}\boldsymbol{\omega}|^2}{\boldsymbol{f}^H\Omega_1\boldsymbol{f}} = \frac{|\boldsymbol{f}^H\bar{H}\boldsymbol{\omega}|^2}{\boldsymbol{\omega}^H\Omega_2\boldsymbol{\omega}} \\ \text{s.t.} \ & \text{(9b), (9c), (9d).} \end{aligned} \tag{18}$$

The reformulated nonconvex fractional problem $\mathcal{P}2$ is still tough to solve. The nonconvex unit-modulus constraint of the IRS phase shift design (9d) is intractable. In addition, the expectation term in the objective function is computationally expensive without instantaneous CSI.

C. Outage Probability Minimization Algorithm Design

In this section, an alternating algorithm is proposed to solve the tough problem $\mathcal{P}2$ by sequentially optimizing one of the decision variables while fixing the others.

Given the transceiver beamforming vectors $\boldsymbol{f}$ and $\boldsymbol{\omega}$, we rewrite $\mathcal{P}2$ considering the denominator part of (18) is independent of $\boldsymbol{\Theta}$

$$\begin{aligned} \mathcal{P}3_A: \ \max_{\boldsymbol{\Theta}} \ & |\boldsymbol{f}^H\bar{H}\boldsymbol{\omega}|^2 \\ \text{s.t.} \ & |\theta_m|^2 = 1, \forall m \in \{1,\ldots,M\}. \end{aligned} \tag{19}$$

To handle this quadratic program, the objective function is reformulated

$$\begin{aligned} |\boldsymbol{f}^H\bar{H}\boldsymbol{\omega}|^2 &= |\boldsymbol{f}^H\left(\alpha_d\bar{H}_d + \alpha_r G^H\Theta^H\bar{H}_r\right)\boldsymbol{\omega}|^2 \\ &= \mathrm{tr}\left(\alpha_d\bar{H}_d^H\mathcal{A}\alpha_d\bar{H}_d\mathcal{B}\right) + \mathrm{tr}(\mathcal{C}\boldsymbol{\Theta}) + \mathrm{tr}\left(\boldsymbol{\Theta}^H\mathcal{C}^H\right) \\ &\quad + \mathrm{tr}\left(\boldsymbol{\Theta}^H\mathcal{D}\boldsymbol{\Theta}\mathcal{E}\right) \end{aligned} \tag{20}$$

where some new variables are introduced as $\mathcal{A} = \boldsymbol{f}\boldsymbol{f}^H$, $\mathcal{B} = \boldsymbol{\omega}\boldsymbol{\omega}^H$, $\mathcal{C} = G\mathcal{A}\alpha_d\bar{H}_d\mathcal{B}\alpha_r\bar{H}_r^H$, $\mathcal{D} = \alpha_r\bar{H}_r\mathcal{B}\alpha_r\bar{H}_r^H$, and $\mathcal{E} = G\mathcal{A}G^H$. Note that the first term in (20) is constant. The above auxiliary variables are nonnegative semi-definite matrices and independent with $\boldsymbol{\Theta}$.

By substituting (20) into (19), the objective can be equivalently re-expressed (with the constant term removed)

$$\max_{\boldsymbol{\Theta}} \quad \mathrm{tr}(\mathcal{C}\boldsymbol{\Theta}) + \mathrm{tr}\big(\boldsymbol{\Theta}^H\mathcal{C}^H\big) + \mathrm{tr}\big(\boldsymbol{\Theta}^H\mathcal{D}\boldsymbol{\Theta}\mathcal{E}\big) \triangleq \Gamma(\boldsymbol{\theta}). \tag{21}$$

We define a column vector $\boldsymbol{c} = \mathrm{diag}(\mathcal{C}) \in \mathbb{C}^{M\times 1}$ with $\boldsymbol{c}_m = \mathcal{C}_{m,m}, \forall m \in \{1, \cdots, M\}$. According to the following properties regarding trace operation:

$$\mathrm{tr}(\mathcal{C}\boldsymbol{\Theta}) = \boldsymbol{c}^T\boldsymbol{\theta}, \quad \mathrm{tr}\big(\boldsymbol{\Theta}^H\mathcal{D}\boldsymbol{\Theta}\mathcal{E}\big) = \boldsymbol{\theta}^H\big(\mathcal{D}\odot\mathcal{E}^T\big)\boldsymbol{\theta} \tag{22}$$

it can be inferred that

$$\Gamma(\boldsymbol{\theta}) = \boldsymbol{\theta}^H\big(\mathcal{D}\odot\mathcal{E}^T\big)\boldsymbol{\theta} + \boldsymbol{c}^T\boldsymbol{\theta} + \boldsymbol{\theta}^H\boldsymbol{c}^*. \tag{23}$$

By far, simplifying and rearranging $\mathcal{P}3_A$ yields the following equivalent problem:

$$\mathcal{P}3_{A'}: \max_{\boldsymbol{\theta}} \quad \Gamma(\boldsymbol{\theta}) \quad \text{s.t.} \quad |\theta_m|^2 = 1, \forall m \in \{1, \ldots, M\}. \tag{24}$$

This subproblem can be transformed as a nonconvex QCQP subject to a unit modulus constraint and the optimal IRS phase shift design $\boldsymbol{\Theta}^*$ ($\boldsymbol{\theta}^*$) can be obtained.

For fixed IRS coefficients ($\boldsymbol{\theta}$) and receive beamforming design ($\boldsymbol{\omega}$), $\mathcal{P}2$ is reduced to a transmit beamforming design problem

$$\mathcal{P}3_B: \max_{\boldsymbol{f}} \quad \frac{|\boldsymbol{f}^H\bar{H}\boldsymbol{\omega}|^2}{\boldsymbol{f}^H\Omega_1\boldsymbol{f}} = \frac{\boldsymbol{f}^H\Xi_1\boldsymbol{f}}{\boldsymbol{f}^H\Omega_1\boldsymbol{f}} \quad \text{s.t.} \quad \|\boldsymbol{f}\|^2 \le P_T \tag{25}$$

where $\Xi_1 = \bar{H}\boldsymbol{\omega}\boldsymbol{\omega}^H\bar{H}^H$. This subproblem is a generalized eigenvalue problem and can be solved by employing the generalized eigenvalue–eigenvectors [35].

Finally, with fixed $\boldsymbol{\theta}$ and $\boldsymbol{f}$, $\mathcal{P}2$ is simplified to a receive beamforming design problem as follows:

$$\mathcal{P}3_C: \max_{\boldsymbol{\omega}} \quad \frac{\boldsymbol{\omega}^H\Xi_2\boldsymbol{\omega}}{\boldsymbol{\omega}^H\Omega_2\boldsymbol{\omega}} \quad \text{s.t.} \quad \|\boldsymbol{\omega}\|^2 \le 1 \tag{26}$$

where $\Xi_2 = \bar{H}^H\boldsymbol{f}\boldsymbol{f}^H\bar{H}$. Similarly, this subproblem can be solved by generalized eigenvalue analysis.

The complete procedure for getting the joint design of IRS coefficients and transceiver beamforming is summarized in Algorithm 1 and detailed in our prior work [1].

Algorithm 1: Outage Probability Optimization Algorithm for Solving $\mathcal{P}2$

Input : Statistical CSI $\bar{H}_d$, $\bar{H}_r$. G, κ_d, κ_r, σ_d^2, and σ_r^2.
Output: $\boldsymbol{\omega}^*, \boldsymbol{f}^*$, $\boldsymbol{\Theta}^*$, SNR γ, and P_{out}.
Initialization: Transceiver beamforming ($\boldsymbol{\omega}$,$\boldsymbol{f}$) and IRS coefficients ($\boldsymbol{\Theta}$) design with maximal SNR from L randomizations.
repeat
  Solve (24) and update $\boldsymbol{\Theta}^* = \mathrm{diag}(\boldsymbol{\theta}^*)$;
  Solve (25) and update $\boldsymbol{f}^*$ in the direction of $\lambda_{\max}(\Omega_1^{-1}\Xi_1)$ with amplitude $\sqrt{P_T}$;
  Solve (26) and update $\boldsymbol{\omega}^*$ with $\lambda_{\max}(\Omega_2^{-1}\Xi_2)$;
until *the predefined stopping criterion is satisfied*;

V. Ergodic Capacity Maximization With Statistical CSI

In the presence of CSI uncertainty, the ergodic capacity of our considered system is calculated as

$$C_{\mathrm{erg}} = \mathbb{E}\left\{\log_2\left(1 + \frac{|\boldsymbol{\omega}^H H^H\boldsymbol{f}|^2}{\sigma^2}\right)\right\} \tag{27}$$

where the expectation is taken concerning the time-varying composite channel H. We investigate the ergodic capacity maximization problem, which is formulated as

$$\mathcal{P}4: \max_{\boldsymbol{\omega},\boldsymbol{f},\boldsymbol{\Theta}} \quad C_{\mathrm{erg}} \quad \text{s.t.} \quad \text{(9b), (9c), (9d).} \tag{28}$$

Solving problem $\mathcal{P}4$ is a challenging task because of two reasons. First, an exact analytical expression of the objective function (27) is not solvable. The computational complexity of implicit expressions of ergodic capacity increases with the number of transceiver antennas, which becomes prohibitively high for massive MIMO cases. Second, the nonconvex unit-modulus constraint is intricate. To handle this issue, we investigate the ergodic capacity based on approximations according to Jensens inequality.

Note that $|\boldsymbol{\omega}^H H^H\boldsymbol{f}|^2 = \mathrm{tr}(H^H\boldsymbol{f}\boldsymbol{f}^H H\boldsymbol{\omega}\boldsymbol{\omega}^H)$ is convex of channel H, and $\log(\cdot)$ is strictly concave and increasing over $\mathbb{R}_+$. According to Jensens inequality [36], the objective function in $\mathcal{P}4$ is upper bounded as follows:

$$\mathbb{E}\left\{\log_2\left(1 + \frac{|\boldsymbol{\omega}^H H^H\boldsymbol{f}|^2}{\sigma^2}\right)\right\} \le \log_2\left(1 + \frac{\mathbb{E}\{|\boldsymbol{\omega}^H H^H\boldsymbol{f}|^2\}}{\sigma^2}\right). \tag{29}$$

We establish an upper-bound problem

$$\mathcal{P}5: \max_{\boldsymbol{\omega}\boldsymbol{f},\boldsymbol{\Theta}} \quad \mathbb{E}\left\{|\boldsymbol{\omega}^H H^H\boldsymbol{f}|^2\right\} \overset{a}{=} \mu_X^2 + \sigma_X^2 \quad \text{s.t.} \quad \text{(9b), (9c), (9d)} \tag{30}$$

where $\overset{a}{=}$ comes from Proposition 2. Let C_{erg}, C_1 denote the optimum obtained by solving $\mathcal{P}4$ and $\mathcal{P}5$, respectively. It implies that $C_{\mathrm{erg}} \le \log_2(1 + [C_1/\sigma^2]) \triangleq C_{ub}$.

A. Upper Bound of Ergodic Capacity

We target on solving an upper bound of the ergodic capacity in $\mathcal{P}5$. According to Proposition 3, σ_X^2 is dependent on $\boldsymbol{f}$ and $\boldsymbol{\omega}$, but nonrelated to $\boldsymbol{\Theta}$. This implies that with given $\boldsymbol{f}$ and $\boldsymbol{\omega}$, $\mathcal{P}5$ is degraded into

$$\mathcal{P}5_A: \max_{\boldsymbol{\Theta}} \quad \mu_X^2 = |\boldsymbol{f}^H\bar{H}\boldsymbol{\omega}|^2 \quad \text{s.t.} \quad |\theta_m|^2 = 1, \forall m \in \{1, \ldots, M\}. \tag{31}$$

Note that $\mathcal{P}5_A$ is the same as $\mathcal{P}3_A$, and the optimal IRS phase shift matrix $\boldsymbol{\Theta}^*$, obtained by solving the outage probability minimization problem also fits well with an upper bound of the ergodic capacity maximization solution.

We investigate the transceiver beamforming design by calculating the upper bound of the ergodic capacity in $\mathcal{P}5$ with an

Algorithm 2: Ergodic Capacity Optimization Algorithm for Solving $\mathcal{P}5$

Input : Statistical CSI $\bar{H}_d$, $\bar{H}_r$. G, κ_d, κ_r, σ_d^2, and σ_r^2.
Output: $\boldsymbol{\omega}^*, \boldsymbol{f}^*$, $\boldsymbol{\Theta}^*$, SNR γ, and C_{ub}.
Initialization: Transceiver beamforming $(\boldsymbol{\omega}, \boldsymbol{f})$ and IRS coefficients $(\boldsymbol{\Theta})$ design with maximal SNR from L randomizations.
repeat
  Solve (31) and update $\boldsymbol{\Theta}^* = \text{diag}(\boldsymbol{\theta}^*)$;
  Solve (32) and update $\boldsymbol{f}^*$ in the direction of $\lambda_{\max}(\Upsilon_1)$ with amplitude $\sqrt{P_T}$;
  Solve (33) and update $\boldsymbol{\omega}^*$ with $\lambda_{\max}(\Upsilon_2)$.
until *the predefined stopping criterion is satisfied*;

alternative optimization method. First, with the fixed receiver beamformer $\boldsymbol{\omega}$, the optimization problem boils down to

$$\mathcal{P}5_B: \max_{\boldsymbol{f}} \quad \mu_X^2 + \sigma_X^2 = \boldsymbol{f}^H \Upsilon_1 \boldsymbol{f} \quad \text{s.t.} \quad \|\boldsymbol{f}\|^2 \le P_T. \tag{32}$$

Then, with obtained transmitter beamformer $\boldsymbol{f}$, the optimization problem is simplified as

$$\mathcal{P}5_C: \max_{\boldsymbol{\omega}} \quad \mu_X^2 + \sigma_X^2 = \boldsymbol{\omega}^H \Upsilon_2 \boldsymbol{\omega} \quad \text{s.t.} \quad \|\boldsymbol{\omega}\|^2 \le 1. \tag{33}$$

Note that $\Upsilon_1 = \Xi_1 + \Omega_1$ and $\Upsilon_2 = \Xi_2 + \Omega_2$. The optimal solution of transceiver beamforming is to find the eigenvector associated with the largest eigenvalue related to Υ_1 and Υ_2, respectively. Particularly, let ς and ζ be the eigenvector of Υ_1 and Υ_2 corresponding to the largest eigenvalue. The optimal BS beamforming vector is $\boldsymbol{f}^* = \sqrt{P_T}\varsigma$, and the optimal MR beamforming vector is $\boldsymbol{\omega}^* = \zeta$, respectively.

The presented algorithm to solve the upper bound of the ergodic capacity maximization problem $\mathcal{P}5$ is detailed in Algorithm 2.

B. Jensen's Approximation of Ergodic Capacity

To further investigate the influence of the IRS on the system performance improvement with the ideal transceiver beamforming design, we utilize the trace properties again and relax the received signal power

$$\begin{aligned} |\boldsymbol{\omega}^H H^H \boldsymbol{f}|^2 &= \text{tr}\big(\boldsymbol{\omega}^H H^H \boldsymbol{f}\boldsymbol{f}^H H \boldsymbol{\omega}\big) \\ &\le \lambda_{\max}\big(\boldsymbol{\omega}\boldsymbol{\omega}^H\big)\text{tr}\big(H^H \boldsymbol{f}\boldsymbol{f}^H H\big) \\ &\le \lambda_{\max}\big(\boldsymbol{\omega}\boldsymbol{\omega}^H\big)\lambda_{\max}\big(\boldsymbol{f}\boldsymbol{f}^H\big)\text{tr}\big(H^H H\big) \overset{b}{\le} P_T \text{tr}\big(H^H H\big) \end{aligned} \tag{34}$$

where $\overset{b}{\le}$ comes from (9b) and (9c), which means that $\lambda_{\max}(\boldsymbol{f}^H\boldsymbol{f}) \le P_T$, and $\lambda_{\max}(\boldsymbol{\omega}^H\boldsymbol{\omega}) \le 1$, respectively.

By this way, we can find that

$$\mathbb{E}\Big\{|\boldsymbol{\omega}^H H^H \boldsymbol{f}|^2\Big\} \le P_T \mathbb{E}\big\{\text{tr}\big(H^H H\big)\big\} \overset{c}{=} P_T \Lambda(\boldsymbol{\Theta}) \triangleq C_2 \tag{36}$$

where $\overset{c}{=}$ comes from the mathematical manipulations in (35), shown at the bottom of the page, where $\mathbb{E}\{\tilde{H}_d^H \tilde{H}_d\} = \sigma_d^2$ and $\mathbb{E}\{\tilde{H}_r^H \tilde{H}_r\} = \sigma_r^2$.

It can be obtained that $C_{\text{erg}} \le C_{ub} \le C_{\text{Jensen}} \triangleq \log_2(1 + [C_2/\sigma^2])$. Herein C_{Jensen} mainly depends on the IRS phase-shift matrix $\boldsymbol{\Theta}$, thus we focus on the following optimization problem:

$$\mathcal{P}6: \max_{\boldsymbol{\Theta}} \quad \Lambda(\boldsymbol{\Theta}) \quad \text{s.t.} \quad |\theta_m|^2 = 1, \forall m \in \{1, \ldots, M\}. \tag{37}$$

Problem $\mathcal{P}6$ can be readily solved using the homogeneous QCQP transformation [15], which is addressed in the same way as Problem $\mathcal{P}3_A$. C_{Jensen} can be obtained after acquiring the optimal values for $\boldsymbol{\Theta}^*$ and Λ^* and illustrates Jensen's approximation upper bound of the ergodic capacity.

VI. Performance Evaluation

In this section, simulation results are provided to evaluate the proposed algorithms in terms of the outage performance and the ergodic capacity. The transmit power and the horizontal BS-IRS distance are set to be $P_T = 42$ dBm and $d_0 = 150$ m, if not specified. The train runs at an average speed of 360 km/h and the system performance is averaged over the cell coverage. The path loss in LoS components $\bar{H}_d$ and $\bar{H}_r$ are modeled as follows [30]:

$$\text{PL} = \alpha_0 + 10\beta_0 \log_{10}\big(d_{\text{Tx,Rx}}\big) \tag{38}$$

where α_0, β_0, and $d_{\text{Tx,Rx}}$ denote the interception, slope, and link distance, respectively. More details are available in [30]. Each simulation composes of 10^3 trails and $L = 100$ random initialization. Unless otherwise specified, the main parameters are listed in Table I.

A. Outage Probability Minimization Performance

To validate the performance of the proposed Algorithm 1, we present the following benchmark schemes for comparison.

1) *Perfect CSI (P-CSI):* The presented Algorithm 1 is performed under the assumption that perfect instantaneous CSI of all corresponding channels is available.
2) *Without IRS:* We consider a traditional system without IRS then minimize the outage probability.

$$\begin{aligned} \mathbb{E}\big\{\text{tr}\big(H^H H\big)\big\} &= \text{tr}\big(\mathbb{E}\big\{H^H H\big\}\big) = \text{tr}\big(\mathbb{E}\big\{H_d^H H_d + G^H \boldsymbol{\Theta}^H H_r H_d^H + H_d H_r^H \boldsymbol{\Theta} G + G^H \boldsymbol{\Theta}^H H_r H_r^H \boldsymbol{\Theta} G\big\}\big) \\ &= \text{tr}\big(\mathbb{E}\big\{H_d^H H_d\big\}\big) + \text{tr}\big(\mathbb{E}\big\{G^H \boldsymbol{\Theta}^H H_r H_d^H\big\}\big) + \text{tr}\big(\mathbb{E}\big\{H_d H_r^H \boldsymbol{\Theta} G\big\}\big) + \text{tr}\big(\mathbb{E}\big\{G^H \boldsymbol{\Theta}^H H_r H_r^H \boldsymbol{\Theta} G\big\}\big) \\ &= \text{tr}\big(\bar{H}_d^H \bar{H}_d\big) + \text{tr}\big(\mathbb{E}\big\{\tilde{H}_d^H \tilde{H}_d\big\}\big) + \text{tr}\big(G^H \boldsymbol{\Theta}^H \bar{H}_r \bar{H}_d^H\big) + \text{tr}\big(\bar{H}_d \bar{H}_r^H \boldsymbol{\Theta} G\big) + \text{tr}\big(\boldsymbol{\Theta} G G^H \boldsymbol{\Theta}^H \big(\bar{H}_r \bar{H}_r^H + \mathbb{E}\big\{\tilde{H}_r \tilde{H}_r^H\big\}\big)\big) \triangleq \Lambda(\boldsymbol{\Theta}) \end{aligned} \tag{35}$$

TABLE I
SIMULATION PARAMETERS

Parameter	Symbol	Value
Carrier frequency	f_c	32 GHz
System bandwidth	W	500 MHz
Noise power density	N_0	–174 dBm/Hz
Height of BS	h_{BS}	10 m
Height of MR	h_{MR}	2.5 m
Height of IRS	h_{IRS}	2.5 m
BS coverage radius	R	600 m
Number of BS antennas	N_{BS}	32
Number of MR antennas	N_{MR}	8
Rician K-factors	κ_d, κ_r	10 dB
SNR threshold	γ_{th}	5 dB
Termination criteria	ϵ	10^{-3}

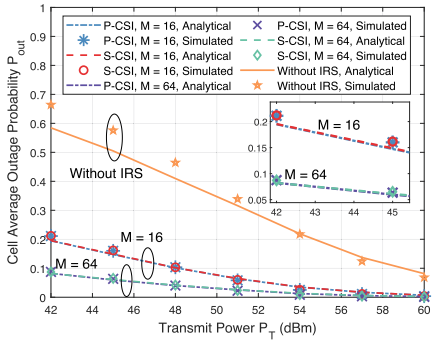

Fig. 2. Outage probability performance with respect to the transmit power.

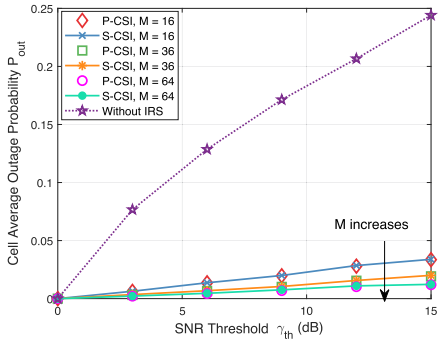

Fig. 3. Outage probability performance with respect to SNR thresholds.

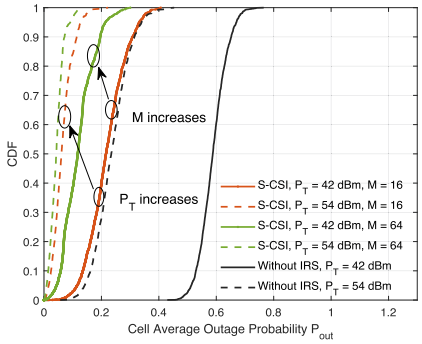

Fig. 4. CDF of the outage probability with respect to the transmit power.

Algorithm 1 is labeled as Statistical CSI (S-CSI) for short.

To verify the analytical accuracy, we consider the above schemes executed under the following two conditions.

1) *Analytical Results:* The outage probability is calculated based on the theoretical analysis of the propositions.
2) *Simulated Results:* The outage probability is achieved by Monte Carlo simulation (all simulations are statistically averaged over a large number of independent runs).

We evaluate the ergodic capacity by the effective capacity C_{eff} multiplied by the nonoutage probability since data is only correctly received on $1 - P_{\text{out}}$ transmissions

$$C_{\text{eff}} \triangleq (1 - P_{\text{out}}) C_{\text{erg}}. \tag{39}$$

Fig. 2 shows the outage probability averaged over the cell with respect to transmit power. As observed, the analytical results agree with the simulation results. This observation validates the accuracy of the closed-form expression of the outage probability derived in Proposition 3. The curves denoted by "S-CSI" and "P-CSI" yield nearly the same outage probability. Thus, the proposed outage probability minimization algorithm can be generalized to the problems when statistical knowledge of CSI can be exploited. As expected, the increasing transmit power limits P_T decrease the SINR outage probability P_{out} since the received signal power at MR rises. Besides, P_{out} decreases as M increases, which demonstrates that the number of IRS reflecting elements is positively related to the regulating ability on EM environmental conditions.

Fig. 3 shows the impact of SNR thresholds γ_{th} on the outage performance. Intuitively, raising SNR thresholds at the receiver side incurs a higher outage probability. It is due to the receiver requiring stronger received signal strength to satisfy a higher SNR threshold, thus more susceptible to outage events. Apparently, the performance gaps between the IRS-assisted system and the system without IRS rise with enlarging SNR thresholds. By comparing the IRS element settings as $M = \{16, 36, 64\}$, the outage probability is decreased as predicted with increasing M, which indicates that the composite channel is highly improved.

Fig. 4 shows the impact of transmit power on the CDF of the outage probability. The black lines denote the performance of the system without IRS. The solid and dashed lines indicate the performance of the proposed S-CSI algorithm with $P_T = 42$ dBm and $P_T = 54$ dBm, respectively. As observed, enlarging transmit power P_T or the IRS element number M reduces the outage probability P_{out}. With $P_T = 42$ dBm and $M = 16$, the cumulative probability of $P_{\text{out}} \leq 0.2$ is about 40%. When enlarging $P_T = 54$ dBm or increasing $M = 64$, the cumulative probability of $P_{\text{out}} \leq 0.2$ rises up to 99.68% and 90%, respectively. In comparison with the system without IRS ($P_T = 54$ dBm, black dashed line), the IRS-assisted system ($P_T = 42$ dBm and $M = 16$, red solid line) achieves a slightly lower outage probability with a narrow gap. It demonstrates that the IRS-assisted system can provide resilience against visibility outages with efficient power saving (around 12 dBm).

Fig. 5 shows the impact of SNR thresholds on the CDF of the outage probability. The dashed and solid lines represent the outage probability distribution obtained by the proposed S-CSI scheme and the scheme without IRS, respectively. The blue, red, and green dashed curves depict the outage performance of the proposed S-CSI scheme against SNR thresholds when $\gamma_{th} = \{0, 9, 15\}$ dB and $M = 36$, respectively. As observed,

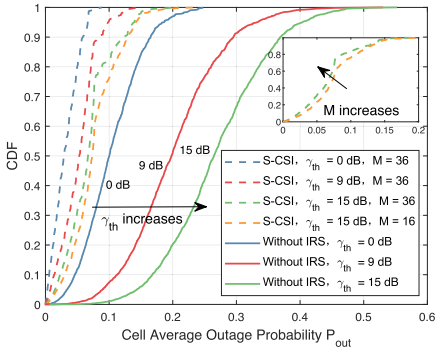

Fig. 5. CDF of the outage probability with respect to SNR thresholds.

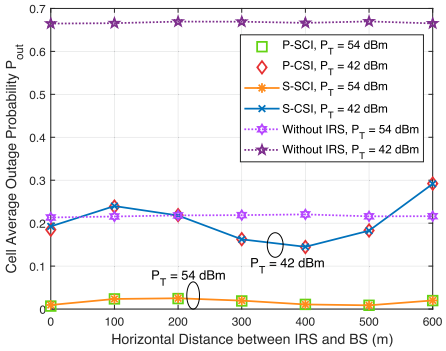

Fig. 6. Outage probability performance with respect to the IRS deployment.

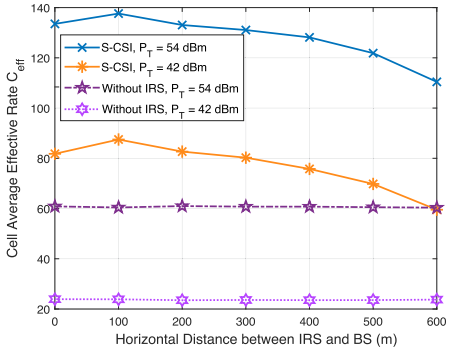

Fig. 7. Effective rate performance with respect to the IRS deployment.

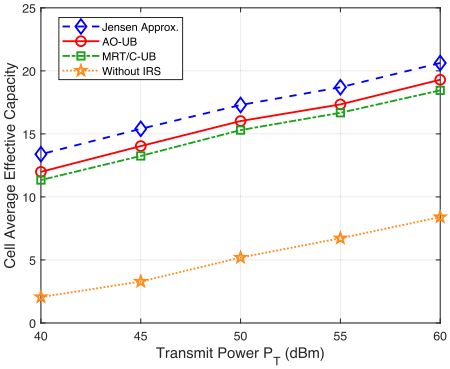

Fig. 8. Effective capacity performance with respect to the transmit power.

the cumulative probabilities of $P_{\text{out}} \leq 0.1$ with $\gamma_{th} = \{0, 9, 15\}$ dB reaches up to 1, 95%, and 81.7%, respectively. The yellow dashed line plots the outage probability attained with $\gamma_{th} = 15$ dB, $M = 16$. By comparing the yellow and green lines, P_{out} decreases as M increases since a better wireless propagation environment is constructed.

Fig. 6 shows the impact of the IRS deployment on the outage performance. The value of the horizontal BS-IRS distance d_0 ranges from 0 to 600 (m). It is worth noting that P_{out} first increases then decreases to a nadir around $d_0 = 400$ m with $P_T = 42$ dBm (or 500 m with $P_T = 54$ dBm), after that the outage probability climbs again. By comparing the outage probability between the IRS-assisted system with $P_T = 42$ dBm and the system without IRS with $P_T = 54$ dBm, we observe that the IRS leads to power saving (around 12 dBm in this simulation settings).

Fig. 7 shows the cell average effective rate with respect to the IRS deployment. As d_0 increases, C_{eff} of the proposed S-CSI algorithm increases at first and then descends, following a unimodal distribution. The peak rate arrives at $d_0 = 100$ m, and C_{eff} closes at its lowest value when IRSs are deployed at the cell edge. By comparing the proposed S-CSI algorithm with $P_T = 42$ dBm and the system without IRS with $P_T = 54$ dBm, it shows that the proposed algorithm significantly boosts the system efficacy and efficiently saves power consumption.

B. Ergodic Capacity Maximization Performance

To characterize the spectrum efficiency of the IRS-assisted system, we investigate the ergodic capacity in terms of channel uncertainty. The simulation experiments are carried out based on the following schemes.

1) *Jensen's Approximation (Jensen Approx.):* Refers to Jensen's Approximation of ergodic capacity C_{Jensen}, obtained by solving Problem $\mathcal{P}6$ with optimal IRS phase-shift matrix design.
2) *Alternative Optimization-Based Upper Bound (AO-UB):* Refers to the ergodic capacity upper bound C_{ub}, obtained from Algorithm 2 with optimal transceiver beamforming vectors and IRS phase-shift matrix design.
3) *Maximum-Ratio Transmission/Combining-Based Upper Bound (MRT/C-UB):* Refers to the ergodic capacity upper bound obtained by assuming the optimal transmitter/receiver beamformer with the maximum-ratio transmission/combining method [37].
4) *Without IRS:* Refers to the ergodic capacity obtained by solving the ergodic capacity maximization problem in the HST system without IRS.

Fig. 8 shows the effective capacity averaged over the whole cell with respect to the transmit power. It is observed that the enlarging transmit power leads to higher received power and larger effective capacity. With $P_T = 40$ dBm, the effective capacity of the system without IRS is around 20% of the IRS-assisted system with MRT/C-UB approach. In particular, the Jensen's approximation significantly outperforms other benchmark schemes, due to the irrespective of transceiver beamforming. The effective capacity with AO-UB is lower than that with Jensen's approximation, which shows a closer bound. Moreover, the AO-UB method is superior to the MRT/C-UB

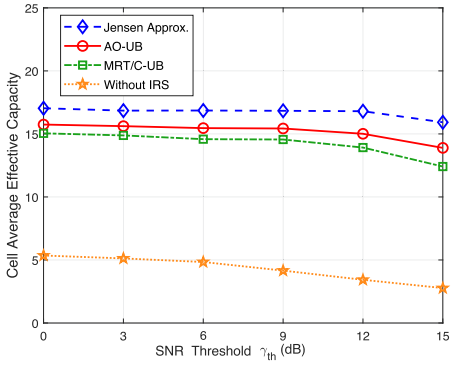

Fig. 9. Effective capacity performance with respect to SNR thresholds.

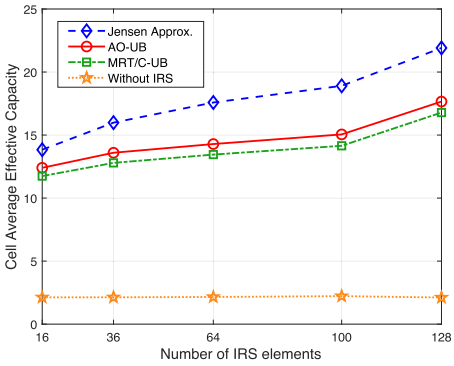

Fig. 10. Effective capacity performance with respect to the number of IRS elements.

in terms of the ergodic capacity, indicating the inferiority of the maximum-ratio-based transceiver beamforming.

Fig. 9 shows the impact of the SNR threshold on the cell average effective capacity. The increment of the SNR threshold indicates higher requirements on the received signal and results in more outage events. We can observe that the IRS-assisted systems are insensitive to the SNR threshold while the system without IRS is more susceptible to the rising SNR threshold. Meanwhile, the performance gap among the schemes in IRS-assisted systems first remains stable and then rises slightly with the SNR threshold.

As shown in Fig. 10, the impact of the number of IRS reflecting elements on the cell average effective capacity is presented. As observed, the system without IRS remains steady in performance and acts as a benchmark. All schemes assisted with IRS show significant performance enhancement with more reflecting elements due to the propagation environment improvement, which resembles the results in the outage minimization performance.

Fig. 11 plots the impact of Rician K-factors on the cell average effective capacity. A larger Rician K-factor implies stronger LoS component and better channel quality. The direct link and reflection link are assumed with the same Rician K-factor, $\kappa_d = \kappa_r$ [36]. If $\kappa_d \to \infty$, the power of the NLoS component can be omitted and the channel model converges to a deterministic LoS channel. If $\kappa_d \to 0$, the channel model reduces to the Rayleigh channel without the LoS component. The effective capacity of each algorithm improves with the Rician K-factor until it reaches the maximum. The proposed

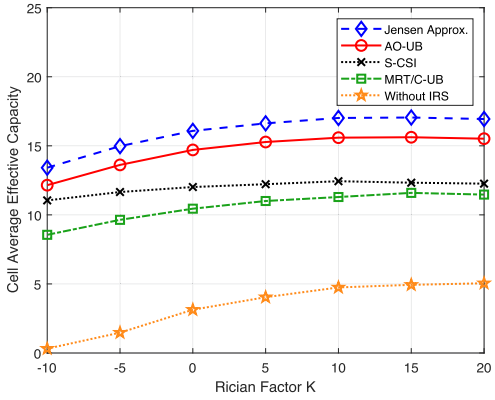

Fig. 11. Effective capacity performance with respect to the Rician K-factor.

Algorithm 1 with the outage probability minimization achieves lower effective capacity than that of the proposed Algorithm 2 with ergodic capacity maximization.

VII. Conclusion

In this article, we have investigated an IRS-assisted downlink HST MIMO communication system with statistical CSI in terms of the outage probability and the ergodic capacity. In particular, the closed-form expression of the outage probability is derived with a generalized Marcum Q-function and the formulated outage probability minimization problem is solved based on the generalized eigenvalue–eigenvectors. The upper bound and Jensen's approximation of the ergodic capacity are analyzed and provided. Theoretical and simulation results have demonstrated the superior performance of the IRS-enhanced system and the optimal configuration by properly adjusting the transceiver beamforming vectors and tuning the IRS phase shift matrix with statistical CSI. This work provides insights to similar scenarios with statistical CSI. For future work, to characterize the fundamental limit of IRS-aided HST communication networks, we extend to the multiuser scenario and manage introduced interference on the system performance.

Appendix A
Proof of Proposition 1

By substituting (3) and (5) into (7), we have

$$\begin{aligned} H &= H_d + G^H \boldsymbol{\Theta}^H H_r \\ &= \left(\alpha_d \bar{H}_d + \alpha_r G^H \Theta^H \bar{H}_r\right) + \left(\beta_d \tilde{H}_d + \beta_r G^H \Theta^H \tilde{H}_r\right) \end{aligned} \quad (40)$$

where $\alpha_d = \sqrt{(\kappa_d/[\kappa_d+1])}$, $\beta_d = \sqrt{(1/[\kappa_d+1])}$, $\alpha_r = \sqrt{(\kappa_r/[\kappa_r+1])}$, and $\beta_r = \sqrt{(1/[\kappa_r+1])}$.

Specifically, $\bar{H} \triangleq \mathbb{E}\{H\} = \alpha_d \bar{H}_d + \alpha_r G^H \Theta^H \bar{H}_r$. It is worth noting that LoS components of both direct and reflection links rest on transceiver distances, and the first part of (40) is deterministic with MR's location information. Since elements of NLoS components of both direct and reflection links obey CSCG distributions with zero mean and variance σ_d^2 (σ_r^2), the second component of (40) obeys Gaussian distribution.

Let $H_{i,j}$ denote the ith row, jth column element of H. The corresponding expectation value is expressed as

$$\begin{aligned}\mu_{i,j} &\triangleq \mathbb{E}\{H_{i,j}\} \\ &= \underbrace{\mathbb{E}\{\alpha_d \bar{H}_d + \alpha_r G^H \Theta^H \bar{H}_r\}_{i,j}}_{\text{deterministic term}} \\ &\quad + \mathbb{E}\{\beta_d \tilde{H}_d + \beta_r G^H \Theta^H \tilde{H}_r\}_{i,j} \\ &= \left(\alpha_d \bar{H}_d + \alpha_r G^H \Theta^H \bar{H}_r\right)_{i,j} + \beta_d \mathbb{E}\{\tilde{H}_d\}_{i,j} \\ &\quad + \beta_r G^H \Theta^H \mathbb{E}\{\tilde{H}_r\}_{i,j} \\ &= \alpha_d \left(\bar{H}_d\right)_{i,j} + \alpha_r \left(G^H \boldsymbol{\Theta}^H \bar{H}_r\right)_{i,j}. \end{aligned} \tag{41}$$

The variance of $H_{i,j}$ can be calculated by

$$\begin{aligned}\sigma_{i,j}^2 &\triangleq \mathrm{var}\{H_{i,j}\} \\ &= \underbrace{\mathrm{var}\{\alpha_d \bar{H}_d + \alpha_r G^H \Theta^H \bar{H}_r\}_{i,j}}_{\text{deterministic term with 0 variance}} \\ &\quad + \mathrm{var}\{\beta_d \tilde{H}_d + \beta_r G^H \Theta^H \tilde{H}_r\}_{i,j} \\ &= \beta_d^2 \mathrm{var}\{\tilde{H}_d\}_{i,j} + \beta_r^2 \mathrm{var}\{G^H \Theta^H \tilde{H}_r\}_{i,j} \\ &= \beta_d^2 \sigma_d^2 + \beta_r^2 \|G_{(:,i)}\|^2 \sigma_r^2. \end{aligned} \tag{42}$$

Thus, each element of H is proved to obey a complex-valued Gaussian distribution, i.e., $H_{i,j} \sim \mathcal{CN}(\mu_{i,j}, \sigma_{i,j}^2)$.

Appendix B
Proof of Proposition 2

The distribution of the product of the Gaussian variable and deterministic variable, independent from each other, is shown to be Gaussian. According to Proposition 1, each element of the composite channel H obeys a complex Gaussian distribution. The transceiver beamforming vectors $\boldsymbol{f}$ and $\boldsymbol{\omega}$ are deterministic and to be calculated. Based on the analysis above, $X \triangleq \boldsymbol{f}^H H \boldsymbol{\omega}$ is also a complex Gaussian variable. The mean and variance of X can be derived as

$$\begin{aligned}\mu_X &= \mathbb{E}\{\boldsymbol{f}^H H \boldsymbol{\omega}\} = \boldsymbol{f}^H \mathbb{E}\{H\} \boldsymbol{\omega} = \boldsymbol{f}^H \bar{H} \boldsymbol{\omega} \\ \sigma_X^2 &= \mathrm{var}\{\boldsymbol{f}^H H \boldsymbol{\omega}\} = \sum_{i=1}^{N_{\mathrm{BS}}} f_i^2 \sum_{j=1}^{N_{\mathrm{MR}}} \omega_j^2 \sigma_{i,j}^2 = \boldsymbol{f}^H \Omega_1 \boldsymbol{f} = \boldsymbol{\omega}^H \Omega_2 \boldsymbol{\omega} \end{aligned} \tag{43}$$

where $\bar{H}_{i,j} = \mu_{i,j}$. Two auxiliary variables are introduced for simplification

$$\begin{aligned}&\Omega_1 = \mathrm{diag}(\boldsymbol{\varpi}), (\boldsymbol{\varpi})_i = \sum_{j=1}^{N_{\mathrm{MR}}} \sigma_{i,j}^2 |\omega_j|^2, \forall i \in \{1, \ldots, N_{\mathrm{BS}}\} \\ &\Omega_2 = \mathrm{diag}(\boldsymbol{\varrho}), (\boldsymbol{\varrho})_j = \sum_{i=1}^{N_{\mathrm{BS}}} \sigma_{i,j}^2 |f_i|^2, \forall j \in \{1, \ldots, N_{\mathrm{MR}}\}. \end{aligned} \tag{44}$$

Therefore, X is proved to obey a complex Gaussian distribution $X \sim \mathcal{CN}(\mu_X, \sigma_X^2)$.

References

[1] M. Gao, B. Ai, Y. Niu, Z. Han, and Z. Zhong, "IRS-assisted high-speed train communications: Outage probability minimization with statistical CSI," in *Proc. IEEE Int. Conf. Commun. (ICC)*, Jun. 2021, pp. 1–6.

[2] B. Ai, A. F. Molisch, M. Rupp, and Z.-D. Zhong, "5G key technologies for smart railways," *Proc. IEEE*, vol. 108, no. 6, pp. 856–893, Jun. 2020.

[3] X. Shen et al., "AI-assisted network-slicing based next-generation wireless networks," *IEEE Open J. Veh. Technol.*, vol. 1, pp. 45–66, 2020.

[4] W. Wu, N. Cheng, N. Zhang, P. Yang, W. Zhuang, and X. Shen, "Fast mmWave beam alignment via correlated bandit learning," *IEEE Trans. Wireless Commun.*, vol. 18, no. 12, pp. 5894–5908, Dec. 2019.

[5] M. Gao et al., "Efficient hybrid beamforming with anti-blockage design for high-speed railway communications," *IEEE Trans. Veh. Technol.*, vol. 69, no. 9, pp. 9643–9655, Sep. 2020.

[6] S. Gong et al., "Toward smart wireless communications via intelligent reflecting surfaces: A contemporary survey," *IEEE Commun. Surveys Tuts.*, vol. 22, no. 4, pp. 2283–2314, 4th Quart., 2020.

[7] Q. Wu and R. Zhang, "Towards smart and reconfigurable environment: Intelligent reflecting surface aided wireless network," *IEEE Commun. Mag.*, vol. 58, no. 1, pp. 106–112, Jan. 2020.

[8] Q. Li, N. Zhang, M. Cheffena, and X. Shen, "Channel-based optimal back-off delay control in delay-constrained industrial WSNs," *IEEE Trans. Wireless Commun.*, vol. 19, no. 1, pp. 696–711, Jan. 2020.

[9] S. Li, L. Bariah, S. Muhaidat, A. Wang, and J. Liang, "Outage analysis of NOMA-enabled backscatter communications with intelligent reflecting surfaces," *IEEE Internet Things J.*, vol. 9, no. 16, pp. 15390–15400, Aug. 2022.

[10] J. Li et al., "Mobility support for millimeter wave communications: Opportunities and challenges," *IEEE Commun. Surveys Tuts.*, vol. 24, no. 3, pp. 1816–1842, 3rd Quart., 2022.

[11] L. You et al., "Network massive MIMO transmission over millimeter-wave and terahertz bands: Mobility enhancement and blockage mitigation," *IEEE J. Sel. Areas Commun.*, vol. 38, no. 12, pp. 2946–2960, Dec. 2020.

[12] Y. Niu, C. Gao, Y. Li, L. Su, and D. Jin, "Exploiting multi-hop relaying to overcome blockage in directional mmWave small cells," *J. Commun. Netw.*, vol. 18, no. 3, pp. 364–374, Jun. 2016.

[13] E. Björnson, Ö. Özdogan, and E. G. Larsson, "Intelligent reflecting surface versus decode-and-forward: How large surfaces are needed to beat relaying?" *IEEE Wireless Commun. Lett.*, vol. 9, no. 2, pp. 244–248, Feb. 2020.

[14] H. Iimori, G. T. F. de Abreu, O. Taghizadeh, R.-A. Stoica, T. Hara, and K. Ishibashi, "Stochastic learning robust beamforming for millimeter-wave systems with path blockage," *IEEE Wireless Commun. Lett.*, vol. 9, no. 9, pp. 1557–1561, Sep. 2020.

[15] Q. Wu and R. Zhang, "Intelligent reflecting surface enhanced wireless network via joint active and passive beamforming," *IEEE Trans. Wireless Commun.*, vol. 18, no. 11, pp. 5394–5409, Nov. 2019.

[16] Y. Chen et al., "Reconfigurable intelligent surface assisted device-to-device communications," *IEEE Trans. Wireless Commun.*, vol. 20, no. 5, pp. 2792–2804, May 2021.

[17] C. Xu et al., "Channel estimation for reconfigurable intelligent surface assisted high-mobility wireless systems," *IEEE Trans. Veh. Technol.*, vol. 72, no. 1, pp. 718–734, Jan. 2023.

[18] B. Zheng, C. You, and R. Zhang, "Intelligent reflecting surface assisted multi-user OFDMA: Channel estimation and training design," *IEEE Trans. Wireless*, vol. 19, no. 12, pp. 8315–8329, Dec. 2020.

[19] P. Wang, J. Fang, H. Duan, and H. Li, "Compressed channel estimation for intelligent reflecting surface-assisted millimeter wave systems," *IEEE Signal Process. Lett.*, vol. 27, pp. 905–909, 2020.

[20] C. Liu, X. Liu, Z. Wei, D. W. K. Ng, and R. Schober, "Scalable predictive Beamforming for IRS-assisted multi-user communications: A deep learning approach," 2022, *arXiv:2211.12644*.

[21] J. Zhang et al., "RIS-aided next-generation high-speed train communications: Challenges, solutions, and future directions," *IEEE Wireless Commun.*, vol. 28, no. 6, pp. 145–151, Dec. 2021.

[22] C. Chen et al., "Joint design of phase shift and transceiver beamforming for intelligent reflecting surface assisted millimeter-wave high-speed railway communications," *IEEE Trans. Veh. Technol.*, vol. 72, no. 5, pp. 6253–6267, 2023.

[23] J. Xu and B. Ai, "When mmWave high-speed railway networks meet reconfigurable intelligent surface: A deep reinforcement learning method," *IEEE Wireless Commun. Lett.*, vol. 11, no. 3, pp. 533–537, Mar. 2022.

[24] T. Li, H. Tong, Y. Xu, X. Su, and G. Qiao, "Double IRSs aided massive MIMO channel estimation and spectrum efficiency maximization for high-speed railway communications," *IEEE Trans. Veh. Technol.*, vol. 71, no. 8, pp. 8630–8645, Aug. 2022.

[25] Z. Huang, B. Zheng, and R. Zhang, "Transforming fading channel from fast to slow: Intelligent refracting surface aided high-mobility communication," *IEEE Trans. Wireless Commun.*, vol. 21, no. 7, pp. 4989–5003, Jul. 2022.
[26] B. Matthiesen, E. Björnson, E. De Carvalho, and P. Popovski, "Intelligent reflecting surface operation under predictable receiver mobility: A continuous time propagation model," *IEEE Wireless Commun. Lett.*, vol. 10, no. 2, pp. 216–220, Feb. 2021.
[27] Z. Ma, Y. Wu, M. Xiao, G. Liu, and Z. Zhang, "Interference suppression for railway wireless communication systems: A reconfigurable intelligent surface approach," *IEEE Trans. Veh. Technol.*, vol. 70, no. 11, pp. 11593–11603, Nov. 2021.
[28] V. Tapio, I. Hemadeh, A. Mourad, A. Shojaeifard, and M. Juntti, "Survey on reconfigurable intelligent surfaces below 10 GHz," *EURASIP J. Wireless Commun. Netw.*, vol. 2021, Sep. 2021, Art. no. 175. [Online]. Available: https://link.springer.com/article/10.1186/s13638-021-02048-5
[29] J. Yang et al., "A geometry-based stochastic channel model for the millimeter-wave band in a 3GPP high-speed train scenario," *IEEE Trans. Veh. Technol.*, vol. 67, no. 5, pp. 3853–3865, May 2018.
[30] D. He et al., "Channel measurement, simulation, and analysis for high-speed railway communications in 5G millimeter-wave band," *IEEE Trans. Intell. Transp. Syst.*, vol. 19, no. 10, pp. 3144–3158, Oct. 2018.
[31] F. Lyu et al., "Characterizing urban vehicle-to-vehicle communications for reliable safety applications," *IEEE Trans. Intell. Transp. Syst.*, vol. 21, no. 6, pp. 2586–2602, Jun. 2020.
[32] S. Yin, A. Baricz, and S. Zhou, "On the monotonicity, log-concavity, and tight bounds of the generalized Marcum and Nuttall Q-functions," *IEEE Trans. Inf. Theory*, vol. 56, no. 3, pp. 1166–1186, Mar. 2010.
[33] D. J. Maširević, "On new formulas for the cumulative distribution function of the noncentral chi-square distribution," *Mediterr. J. Math*, vol. 14, no. 66, pp. 1–13, Mar. 2017.
[34] N. L. Johnson, S. Kotz, and N. Balakrishnan, *Continuous Univariate Distributions*, vol. 2. New York, NY, USA: Wiley, 1995.
[35] A. Khisti and G. W. Wornell, "Secure transmission with multiple antennas I: The MISOME wiretap channel," *IEEE Trans. Inf. Theory*, vol. 56, no. 7, pp. 3088–3104, Jul. 2010.
[36] Y. Han, W. Tang, S. Jin, C. Wen, and X. Ma, "Large intelligent surface-assisted wireless communication exploiting statistical CSI," *IEEE Trans. Veh. Technol.*, vol. 68, no. 8, pp. 8238–8242, Aug. 2019.
[37] J.-C. Chen, "Beamforming optimization for intelligent reflecting surface-aided MISO communication systems," *IEEE Trans. Veh. Technol.*, vol. 70, no. 1, pp. 504–513, Jan. 2021.

Meilin Gao (Member, IEEE) received the Ph.D. degree from Beijing Jiaotong University, Beijing, China, in 2021.

She is currently a Postdoctoral Fellow with Tsinghua University, Beijing. She was a visiting Ph.D. student with the BBCR Group, Department of Electrical and Computer Engineering, University of Waterloo, Waterloo, ON, Canada, from September 2018 to January 2020. Her current research interests include millimeter-wave communications, wireless resource allocation, and mobile-edge caching.

Bo Ai (Fellow, IEEE) received the M.S. and Ph.D. degrees from Xidian University, Xi'an, China, in 2002 and 2004, respectively.

He was with Tsinghua University, Beijing, China, where he was an Excellent Postdoctoral Research Fellow in 2007. He is currently a Professor and an Advisor of Ph.D. candidates with Beijing Jiaotong University, Beijing, and the Deputy Director of the State Key Laboratory of Rail Traffic Control and Safety, Beijing Jiaotong University, and is also currently with the Engineering College, Armed Police Force, Xi'an. He has authored or coauthored six books and 270 scientific research papers, and holds 26 invention patents in his research areas. His interests include the research and applications of orthogonal frequency-division multiplexing techniques, high-power amplifier linearization techniques, radio propagation and channel modeling, global systems for mobile communications for railway systems, and long-term evolution for railway systems.

Dr. Ai has received many awards, such as the Qiushi Outstanding Youth Award by HongKong Qiushi Foundation, the New Century Talents by the Chinese Ministry of Education, the Zhan Tianyou Railway Science and Technology Award by the Chinese Ministry of Railways, and the Science and Technology New Star by the Beijing Municipal Science and Technology Commission. He was a Co-Chair or a Session/Track Chair for many international conferences, such as the 9th International Heavy Haul Conference 2009; the 2011 IEEE International Conference on Intelligent Rail Transportation; HSRCom 2011; the 2012 IEEE International Symposium on Consumer Electronics; the 2013 International Conference on Wireless, Mobile and Multimedia; IEEE Green HetNet 2013; and the IEEE 78th Vehicular Technology Conference 2014. He is an Associate Editor of IEEE TRANSACTIONS ON CONSUMER ELECTRONICS and an Editorial Committee Member of the *Wireless Personal Communications* journal. He is a Fellow of the Institution of Engineering and Technology.

Yong Niu (Senior Member, IEEE) received the B.E. degree in electrical engineering from Beijing Jiaotong University, Beijing, China, in 2011, and the Ph.D. degree in electronic engineering from Tsinghua University, Beijing, in 2016.

From 2014 to 2015, he was a Visiting Scholar with the University of Florida, Gainesville, FL, USA. He is currently an Associate Professor with the State Key Laboratory of Rail Traffic Control and Safety, Beijing Jiaotong University. His research interests are in the areas of networking and communications, including millimeter-wave communications, device-to-device communication, medium access control, and software-defined networks.

Dr. Niu was the recipient of the 2018 International Union of Radio Science Young Scientist Award. He received the Ph.D. National Scholarship of China in 2015, the Outstanding Ph.D. Graduates and Outstanding Doctoral Thesis of Tsinghua University in 2016, the Outstanding Ph.D. Graduates of Beijing in 2016, and the Outstanding Doctorate Dissertation Award from the Chinese Institute of Electronics in 2017. He has served as a Technical Program Committee Member for IWCMC 2017, VTC2018-Spring, IWCMC 2018, INFOCOM 2018, and ICC 2018. He was the Session Chair for IWCMC 2017.

Qihao Li (Member, IEEE) received the M.Sc. degree in information and communication technology from the University of Agder, Kristiansand, Norway, in 2013, and the Ph.D. degree from the Department of Electrical and Computer Engineering, University of Oslo, Oslo, Norway, in 2019.

In 2016, he was a Visiting Researcher with the Department of Electrical and Computer Engineering, University of Waterloo, Waterloo, ON, Canada, where he was a Postdoctoral Fellow in 2020. He is currently a Lecturer with the School of Electrical Engineering and Intelligentization, Dongguan University of Technology, Dongguan, China. His current research focuses on industrial wireless sensor network, optimal control and optimization, and wireless network security and localization.

Dr. Li served as a member of Technical Program Committee for IEEE Globecom'19–22, IEEE ICC'19–22, EEE CIC ICCC'17–22, EuCAP'2019, and BDEC-SmartCity'18.

Zhu Han (Fellow, IEEE) received the B.S. degree in electronic engineering from Tsinghua University, Beijing, China, in 1997, and the M.S. and Ph.D. degrees in electrical and computer engineering from the University of Maryland at College Park, College Park, MD, USA, in 1999 and 2003, respectively.

From 2000 to 2002, he was a Research and Development Engineer with JDSU, Germantown, MD, USA. From 2003 to 2006, he was a Research Associate with the University of Maryland at College Park. From 2006 to 2008, he was an Assistant Professor with Boise State University, Boise, ID, USA. He is currently a John and Rebecca Moores Professor with the Electrical and Computer Engineering Department as well as with the Computer Science Department, University of Houston, Houston, TX, USA. His main research targets on the novel game-theory-related concepts critical to enabling efficient and distributive use of wireless networks with limited resources. His other research interests include wireless resource allocation and management, wireless communications and networking, quantum computing, data science, smart grid, security, and privacy.

Dr. Han received an NSF Career Award in 2010, the Fred W. Ellersick Prize of the IEEE Communication Society in 2011, the EURASIP Best Paper Award for the *Journal on Advances in Signal Processing* in 2015, the IEEE Leonard G. Abraham Prize in the field of Communications Systems (best paper award in IEEE JSAC) in 2016, and several Best Paper Awards in IEEE conferences. He is also the winner of the 2021 IEEE Kiyo Tomiyasu Award, for outstanding early to mid-career contributions to technologies holding the promise of innovative applications, with the following citation: "for contributions to game theory and distributed management of autonomous communication networks." He was an IEEE Communications Society Distinguished Lecturer from 2015 to 2018 and has been an ACM Distinguished Member since 2019. He has been a 1% Highly Cited Researcher since 2017 according to Web of Science. He has been an AAAS Fellow since 2019.

Zhangdui Zhong (Fellow, IEEE) received the B.S. and M.S. degrees from Beijing Jiaotong University (BJTU), Beijing, China, in 1983 and 1988, respectively.

He is currently a Professor and a Chief Scientist with the State Key Laboratory of Rail Traffic Control and Safety, BJTU. He is a Director of the Innovative Research Team, Ministry of Education, and a Chief Scientist with the Ministry of Railways in China. His research interests include wireless communications for railways, control theory and techniques for railways, and global system for mobile communications-railway.

Prof. Zhong was a recipient of the Mao Yisheng Scientific Award of China, the Zhan Tianyou Railway Honorary Award of China, and the Top Ten Science/Technology Achievements Award of Chinese Universities.

Xuemin (Sherman) Shen (Fellow, IEEE) received the Ph.D. degree in electrical engineering from Rutgers University, New Brunswick, NJ, USA, in 1990.

He is currently a University Professor with the Department of Electrical and Computer Engineering, University of Waterloo, Waterloo, ON, Canada. His research focuses on network resource management, wireless network security, social networks, 5G and beyond, and vehicular ad hoc and sensor networks.

Dr. Shen received the R.A. Fessenden Award in 2019 from IEEE, Canada, the James Evans Avant Garde Award in 2018 from the IEEE Vehicular Technology Society, and the Joseph LoCicero Award in 2015, and Education Award in 2017 from the IEEE Communications Society. He has also received the Excellent Graduate Supervision Award in 2006 from the University of Waterloo and the Premier's Research Excellence Award in 2003 from the Province of Ontario, Canada. He served as the Technical Program Committee Chair/Co-Chair for the IEEE Globecom'16, the IEEE Infocom'14, the IEEE VTC'10 Fall, and the IEEE Globecom'07, the Symposia Chair for the IEEE ICC'10, the Tutorial Chair for the IEEE VTC'11 Spring, and the Chair for the IEEE Communications Society Technical Committee on Wireless Communications. He was the Editor-in-Chief of the IEEE INTERNET OF THINGS JOURNAL and a Vice President on Publications of the IEEE Communications Society. He is a Registered Professional Engineer of Ontario, Canada, an Engineering Institute of Canada Fellow, a Canadian Academy of Engineering Fellow, a Royal Society of Canada Fellow, a Chinese Academy of Engineering Foreign Fellow, and a Distinguished Lecturer of the IEEE Vehicular Technology Society and Communications Society.

Ning Wang (Member, IEEE) received the B.E. degree in communication engineering from Tianjin University, Tianjin, China, in 2004, the M.A.Sc. degree in electrical engineering from The University of British Columbia, Vancouver, BC, Canada, in 2010, and the Ph.D. degree in electrical engineering from the University of Victoria, Victoria, BC, Canada, in 2013.

He was on the Finalist of the Governor Generals Gold Medal for Outstanding Graduating Doctoral Student with the University of Victoria in 2013. From 2004 to 2008, he was with China Information Technology Design and Consulting Institute as a Mobile Communication System Engineer, specializing in planning and design of commercial mobile communication networks, network traffic analysis, and radio network optimization. He was a Postdoctoral Research Fellow with the Department of Electrical and Computer Engineering, The University of British Columbia from 2013 to 2015. Since 2015, he has been with the School of Information Engineering, Zhengzhou University, Zhengzhou, China, where he is currently an Associate Professor. He also holds adjunct appointments with the Department of Electrical and Computer Engineering, McMaster University, Hamilton, ON, Canada, and with the Department of Electrical and Computer Engineering, University of Victoria. His research interests include resource allocation and security designs of future cellular networks, channel modeling for wireless communications, statistical signal processing, and cooperative wireless communications.

Dr. Wang has served on the technical program committees of international conferences, including the IEEE GLOBECOM, IEEE ICC, IEEE WCNC, and CyberC.